Journal of Inorganic Biochemistry 151 (2015) 1–9

Contents lists available at ScienceDirect

Journal of Inorganic Biochemistry

journal homepage: www.elsevier.com/locate/jinorgbio

The homopentameric chlorite dismutase from *Magnetospirillum* sp.

Diana M. Freire [a,1], Maria G. Rivas [a,b], André M. Dias [a], Ana T. Lopes [a], Cristina Costa [a], Teresa Santos-Silva [a], Sabine Van Doorslaer [c,*], Pablo J. González [a,b,*]

[a] UCIBIO, REQUIMTE, Departamento de Química, Faculdade de Ciências e Tecnologia, Universidade Nova de Lisboa, 2829-516 Caparica, Portugal
[b] Departamento de Física, Facultad de Bioquímica y Ciencias Biológicas, Universidad Nacional del Litoral, Ciudad Universitaria, Paraje El Pozo, S3000ZAA Santa Fe, Argentina
[c] Department of Physics, University of Antwerp, Universiteitsplein 1, B-2610 Wilrijk, Belgium

ARTICLE INFO

Article history:
Received 18 February 2015
Received in revised form 3 July 2015
Accepted 9 July 2015
Available online 15 July 2015

Keywords:
Chlorite dismutase
Enzyme kinetics
X-ray crystallography
EPR spectroscopy
Magnetospirillum
Perchlorate-reducing bacteria

ABSTRACT

Chlorite dismutase (Cld) is a *b*-type heme containing enzyme that catalyzes the reduction of chlorite into chloride plus dioxygen. This enzyme has gained attention because it can be used in the development of bioremediation processes, biosensors, and controlled dioxygen production. In the present work, Cld was purified from *Magnetospirillum* sp. cells cultured anaerobically with acetate/perchlorate until stationary phase. Biochemical, spectroscopic and X-ray crystallography methods showed that Cld from *Magnetospirillum* sp. is a ~140 kDa homopentamer comprising ~27.8 kDa monomers. Preliminary X-ray crystallography studies confirmed the quaternary structure and the presence of one *b*-type heme per monomer. The EPR spectroscopic signature of the as-purified Cld samples is affected by the buffer composition used during the purification. Potassium phosphate buffer is the only buffer that affected neither the spectral nor the kinetic properties of Cld. Kinetic studies in solution revealed that Cld from *Magnetospirillum* sp. decomposes chlorite at high turnover rates with optimal pH 6.0. A temperature below 10 °C is required to avoid enzyme inactivation due to cofactor bleaching during turnover, and to achieve full substrate consumption. Cld kinetic parameters were not affected when kinetic assays were performed in the presence of air or under argon atmosphere, but chloride is a weak mixed inhibitor that modifies the EPR signal of as-prepared samples.

1. Introduction

Chlorinated species, mainly perchlorate (ClO_4^-), chlorate (ClO_3^-) and chlorite (ClO_2^-), have been produced in large scale relatively recently by anthropogenic sources. The main source is the chemical industry, which uses these and related compounds in a wide range of applications [1–3]. The presence of significant concentrations of these oxoanions in the environment exerted a selective pressure on living organisms, favoring the propagation of those which have the ability to, not only withstand the presence of polluting oxochlorates, but also to exploit their oxidative properties (ClO_4^-/Cl^- $E^o = 1.287$ V; ClO_3^-/Cl^- $E^o = 1.03$ V) using them as the final electron acceptors in energy conserving respiratory processes [4,5]. Bacteria with the ability to reduce oxochlorates are known as (per)-chlorate-reducing bacteria [6]. They are capable of coupling the reduction of (per)chlorate into chlorite ($ClO_4^- \rightarrow ClO_3^- \rightarrow ClO_2^-$) with the protons translocating to the cell periplasm, generating a proton motive force (PMF) [7]. The accumulated chlorite anion might be toxic for the cell, but chlorite dismutase (Cld) catalyzes its reduction to innocuous chloride anion (Cl^-) plus dioxygen ($O_{2(g)}$). This reaction is notable as it is the second example (the first was the photosystem II) of an enzyme capable of catalyzing an O—O bond formation [8,9].

Cld has gained attention as it can be used in bioremediation processes either to eliminate chlorite from wastewater or for sensing purposes [10]. The most relevant property from the perspective of using Cld enzymes as a biocatalyst for bioremediation is that it catalyzes chlorite decomposition at high turnover rates. Also, Cld can be used for in situ generation of controlled amounts of $O_{2(g)}$ from chlorite salts either for medicinal applications or for the study of O_2-utilizing enzymes [10–12].

At present, several Clds isolated from the native organism cultured under ClO_4^--reducing conditions or heterologously expressed (in *Escherichia coli* strains) were biochemically and structurally characterized [13–17]. The molecular and kinetic properties of the Clds characterized so far showed that despite the different sources, they share key features which determine substrate specificity and reactivity. In this regard, all of them are homomultimeric complexes and each monomer presents one *b*-type heme with an Fe(III) ion. The only remarkable difference found among all the reported Cld, either with or without a reported crystallographic structure, relates to the protein quaternary structure. Namely, Cld from *Dechloromonas aromatica* [18] and *Candidatus Nitrospira defluvii* [17] are homopentamers; while Cld from *Azospira oryzae* strain GR-1 [19] is a homohexamer. Although no structural data is available, Cld from *Ideonella dechloratans* [15] and

* Corresponding authors.
E-mail addresses: sabine.vandoorslaer@ua.ac.be (S. Van Doorslaer), pgonzalez@fbcb.unl.edu.ar (P.J. González).
[1] Present address: European Molecular Biology Laboratory (EMBL), Notkestraße 85, 22603 Hamburg, Germany.

http://dx.doi.org/10.1016/j.jinorgbio.2015.07.006
0162-0134/

Pseudomonas chloritidismutans [9] are reported as homotetramers, but according to amino acid sequence homology studies these Clds would be homopentamers [10]. On the other hand, Cld from *Nitrobacter winogradskyi* [14], *Klebsiella pneumoniae* [20] and *Cyanothece* sp. PCC7425 [21] are homodimers, probably because they are truncated proteins having a heme-binding domain highly similar to penta- and hexameric Clds, but lacking almost the entire N-terminal domain present in full-length Clds [10].

To date, eight Cld crystallographic structures have been published in the PDB database: one from the *A. oryzae* strain GR-1 in complex with thiocyanate (2.10 Å) [19]; four from *Candidatus N. defluvii* in complex with imidazole (1.85 Å) and cyanide (1.94 Å), and the variants R173A (2.60 Å) and R173K (2.70 Å) [17]; two from *D. aromatica* RCB at pH 6.5 (3.05 Å) and pH 9.0 (3.00 Å) [18]; and one from *N. winogradskyi* (2.10 Å) [14]. In all of these cases, the Cld monomer has an αβ structure comprising two similar structural domains with a ferredoxin-type fold. The iron atom of the heme cofactor is pentacoordinated with the axial position occupied by the imidazole ring of one His residue, in agreement with the high-spin Fe(III) EPR signal observed in the as-isolated Cld samples at pH 6.0–7.0 [15,22].

For the present work, we have isolated the Cld from the Gram-negative alphaproteobacterium *Magnetospirillum* sp. This strain, which was isolated from an activated sludge sample taken from a wastewater treatment plant (Prata et al., submitted for publication), is capable of using perchlorate as electron acceptor when cultured under anaerobic conditions. In addition, this perchlorate-reducing bacterium is highly related to the *Magnetospirillum bellicus* strain VDY^T (ATCC BAA-1730) [23] and relatively distant from magnetosome-forming *Magnetospirillum* species like *Magnetospirillum magneticum*, *Magnetospirillum magnetotacticum*, *Magnetospirillum gryphiswaldense* and *Aquaspirillum polymorphum*. In this manuscript, we report the first purification of Cld from a *Magnetospirillum* strain and its biochemical, kinetic, spectroscopic and structural properties are presented.

2. Materials and methods

2.1. Bacterial strain and culture conditions

Magnetospirillum spp. was cultured in a batch reactor at 37 °C under anaerobic conditions (saturated with argon) using the acetate/perchlorate medium optimized by Prata et al. (submitted for publication). The basal medium (8.9 mM $K_2HPO_4 \cdot 3H_2O$, 7.1 mM NaH_2PO_4, 4.7 mM NH_4Cl, 0.4 mM $MgSO_4 \cdot 7H_2O$) was sterilized (121 °C, 1 atm for 20 min) and then supplemented with 0.1% (v/v) of KL medium (14.4 mM $FeSO_4 \cdot 7H_2O$, 1.7 mM $Na_2MoO_4 \cdot 2H_2O$, 10.3 mM EDTA, 9.7 mM H_3BO_3, 421 μM $NiCl_2 \cdot 6H_2O$ and 570 μM $Na_2SeO_3 \cdot 5H_2O$ dissolved in 1 N HCl), 10.0 mM $NaClO_4$ and 20.0 mM $NaCH_3COO$. The final pH of the medium was 7.0 though in some cases it was necessary to adjust the pH with a sterile 5 N NaOH solution.

2.2. Enzyme purification

Magnetospirillum cells from a 300-L batch culture were collected and then disrupted in a French Press (9000 psi). The total cell extract obtained was centrifuged for 30 min at 16,000 ×*g* and the supernatant was subjected to ultracentrifugation at 180,000 ×*g* for 40 min. The supernatant contained the soluble (cytoplasmic and periplasmic) proteins while the membrane fraction was in the pellet.

Purification of the enzyme through either of the two protocols used in this work was carried out using liquid chromatography techniques (FPLC). All the steps were performed at 4 °C. For the first purification protocol, the soluble extract obtained after ultracentrifugation was dialyzed overnight against 10 mM Tris–HCl pH 7.6 and then loaded onto a DE-52 column equilibrated with the same buffer. Under these conditions Cld eluted with the flow-through. The latter was dialyzed against 5 mM MES pH 6.0, concentrated by ultrafiltration (cutoff 30 K), and then loaded onto a SP-Sepharose-FF equilibrated with the same buffer. Cld eluted at approximately 100 mM NaCl during a linear gradient to 10 mM MES pH 6.0 plus 500 mM NaCl. The Cld-containing fractions were pooled and loaded on a hydroxyapatite column equilibrated with 1 mM potassium phosphate buffer (KPB) pH 8.0. Cld eluted at 75 mM KPB during a linear gradient to 250 mM KPB pH 8.0. Cld fractions were pooled, concentrated by ultrafiltration, and stored at −20 °C.

For the second protocol, the use of buffers having chloride as counter-ion (e.g., Tris–HCl) was avoided. In this case, the soluble extract was dialyzed overnight against 5 mM KPB pH 8.0 and then loaded onto the DE-52 column equilibrated with the same buffer. As in the first protocol, Cld eluted with the flow-through, which was concentrated by ultrafiltration prior to its injection into a Superdex 200 column equilibrated with 50 mM phosphate buffer pH 8.0. After this step, Cld was obtained pure as judged by SDS-PAGE [24]. Pure Cld fractions were pooled, concentrated, and stored at −20 °C.

2.3. Molecular mass determination

The molecular mass of the Cld monomer was determined by analysis of non-digested Cld using MALDI-TOF-MS on a positive linear mode. Oligomer mass was determined through size-exclusion chromatography, using the Superdex 200 column (GE Healthcare) previously calibrated with the standards ovalbumin (43 kDa), conalbumin (75 kDa), aldolase (158 kDa) and ferritin (440 kDa).

2.4. Protein, heme and iron quantification

Total protein concentration was determined using the bicinchoninic acid (BCA) kit from Sigma-Aldrich using bovine serum albumin (BSA) as standard.

The heme content was determined through the pyridine-hemochrome assay. A pure Cld sample (1.7 μM) was incubated with 20% pyridine, 75 mM NaOH and 1.0 mM sodium dithionite. The heme concentration was estimated using the reported molar absorption coefficients $\varepsilon_{418} = 191{,}500\ M^{-1}\ cm^{-1}$ and $\varepsilon_{556} = 38{,}800\ M^{-1}\ cm^{-1}$ [25].

Iron was quantified by Inductively Coupled Plasma-Atomic Emission Spectroscopy (ICP-AES) using a Horiba Jobin-Yvon model Ultima spectrometer equipped with a RF generator of 40.68 MHz and a Czerny–Turner type monochromator. Standard iron solution ranging from 0.02 ppm to 1.0 ppm was prepared using the 23 ICP Multi Element Standard in 5% HNO_3 and 0.2% HF (Reagecon).

2.5. Identification by MALDI-TOF-MS

Samples of pure Cld in solution or extracted from a gel ran under denaturating conditions (SDS-PAGE) were digested using trypsin. The identification was performed by Peptide Mass Fingerprint using MASCOT as search engine with MSDB, NCBInr and SwissProt as databases. Two types of modifications were taken into account to perform the identification: cysteine carbamidomethylation (sample was alkylated using iodoacetamide) as fixed, and methionine oxidation as variable.

2.6. Kinetic studies

The catalytic activity of Cld was measured by ultraviolet spectroscopy following the decay of chlorite at 260 nm in an Agilent spectrophotometer (model 8453 DIODE ARRAY) connected with a LAUDA Ecoline RE104 cooling thermostat. The molar absorption coefficient of chlorite anion at 260 nm is $155.2 \pm 0.6\ M^{-1}\ cm^{-1}$ [26]. Since at 260 nm neither the products (chloride and dioxygen) nor Cld (owing to the very low concentration) absorbs, the absorbance at 260 nm decays to zero when the substrate is fully consumed. To validate this, we verified the stoichiometry of the reaction as described elsewhere [16], quantifying the total amount of dioxygen evolved (with a Clark-type electrode)

and the remaining substrate (by iodometric titrations) in a set of reactions.

The reaction mixture comprising the buffer (50 mM potassium phosphate) and the substrate $NaClO_2$ at the desired concentration (0.025–2.5 mM) was contained in 1 mL quartz cells provided with a very efficient magnetic stirring system which allows a precise determination of the initial substrate consumption rates. The reaction was started by addition of the enzyme (~22 nM). Activity assays were performed at several pH values (5.0–9.0), temperatures (5–50 °C) and gauge pressures (−1 to 3 bar) to determine optimal conditions. The inhibitory effect of the chloride anion was studied using NaCl concentrations of 0, 50, 150 and 300 mM and the competitive and uncompetitive inhibition constants were determined from Dixon and Cornish-Bowden plots (Fig. S1) using the method reported by Cornish-Bowden [27].

2.7. Spectroscopic methods

UV–visible spectra were recorded at room temperature on a SHIMADZU 1800 spectrophotometer. Continuous-wave (CW) EPR spectra were recorded on an X-band CW-EPR spectrometer, Bruker EMX 300, equipped with a double-mode cavity (Model ER4116DM) and a continuous-flow cryostat (Oxford Instruments) that allows working in a temperature range between 4 and 300 K. All the spectra were obtained in non-saturating conditions at 10 K using microwave power, 0.6 mW; modulation amplitude, 0.5 mT and modulation frequency, 100 kHz.

2.8. X-ray crystallography

Initial crystallization conditions were screened using an in-house modified version of the sparse-matrix method of Jancarik & Kim [28], in combination with the commercial Hampton Research (California, USA) Crystal Screen and Crystal Screen 2 using a crystallization robot (*Oryx 8*, Douglas Instruments) at 293 K. Small bright red crystals appeared in several conditions a few hours after setting-up the drops. In order to improve the quality of the obtained crystals several parameters such as temperature (277 K), protein concentration (10 to 30 mg/mL), use of additives (additive screens I and II from Hampton Research), concentration of precipitating agent, and drop volume were varied. Also, micro, macro and streak seeding techniques were tested for crystal optimization although no improvements were observed.

The best crystals were obtained at 277 K using a precipitant solution containing 0.2 M NaCl, 0.1 M phosphate–citrate buffer pH 4.2 and 16% PEG 8 K. The drops were prepared with 2 μL of a 28 mg/mL protein solution, 1 μL of the precipitant solution, 1 μL of 100 mM L-cysteine, and 1 μL of 100 mM potassium thiocyanate. Both L-cysteine and thiocyanate resulted to be very important for diffraction quality. Before freezing in liquid nitrogen, the crystals were soaked in a solution containing 0.2 M NaCl, 0.1 M phosphate–citrate buffer pH 4.2, 20% PEG 8 K, and 15% glycerol.

Complete data sets were collected at PXIII of the Swiss Light Source (SLS, Switzerland). The crystals, which belong to a monoclinic space group ($P2_1$), were measured at a wavelength of 0.9795 Å and diffracted up to 3.0 Å resolution. Data processing was carried out using MOSFLM [29] and SCALA [30] from the CCP4 program suite [31,32] and statistics are summarized in Table 1.

In order to determine the solvent content of the crystals, the Matthews coefficient [33] was calculated using the program MATTHEWS_COEF [34], suggesting the presence of 10–12 molecules in the asymmetric unit and a solvent content of ca. 50%.

Structure determination was carried out by molecular replacement using program Phaser [35] from the CCP4 program suite [31,32] and the atoms coordinates of the Cld from *D. aromatica* RCB at pH 6.5 as template (PDB code: 3Q08) [18]. Cld from *D. aromatica* is arranged as a homopentamer, and a single monomer was used for phasing, excluding the heme cofactors. The position of each monomer was found sequentially in a stepwise procedure. The obtained initial phases yielded a good electron density map where the contour of the protein and the solvent channels could be clearly identified. However, two out of ten monomers in the asymmetric unit presented a weaker electron density. Phase improvement was performed using the program DM [36] (CCP4 program suite [31,32]) with the Phaser solution and using a fraction solvent content of 0.55. Model building and refinement were carried out using COOT [37] and Refmac5 [38] (CCP4 program suite [31,32]).

Table 1
X-ray crystallography data collection statistics. Values in parentheses are for the highest resolution shell.

Crystal	Cld
Beamline	PXIII
Wavelength (Å)	0.979
Space group	$P2_1$
Unit cell (Å)	$a = 78.79$, $b = 150.53$, $c = 133.85$
Matthews parameter (Å^3/Da)	2.7
No. observed reflections	192,521 (27,562)
No. unique reflections	60,320 (8821)
Resolution limits (Å)	59.38–3.00 (3.16–3.00)
Completeness (%)	99.9 (100)
Redundancy	3.2 (3.1)
Average I/σ(I)	13.5 (3.1)
R_{merge}[a] (%)	5.6 (38.2)
R_{pim}[b] (%)	3.8 (25.8)

[a] $R_{merge} = \sum_{hkl}\sum_i |I_i(hkl) - \langle I(hkl)\rangle| / \sum_{hkl}\sum_i I_i(hkl)$, where $I_i(hkl)$ is the integrated intensity of a given reflection and $\langle I(hkl)\rangle$ is the mean intensity of multiple corresponding symmetry-related reflections.

[b] $R_{p.\,i.\,m.} = \sum_{hkl}[1/(N-1)]^{1/2}\sum_i |I_i(hkl) - \langle I(hkl)\rangle| / \sum_{hkl}\sum_i I_i(hkl)$, where $I_i(hkl)$ is the integrated intensity of a given reflection, $\langle I(hkl)\rangle$ is the mean intensity of multiple corresponding symmetry-related reflections and N is the multiplicity of a given reflection.

3. Results and discussion

3.1. Molecular properties

Samples of chlorite dismutase (Cld) purified by any of the two methods described in Section 2.2 were used to produce crystals for protein structure determination through X-ray crystallography. Single-crystals of Cld from *Magnetospirillum* sp. were obtained under many different conditions, but most of these crystals diffracted poorly. The best crystals obtained (Fig. S2) were grown at 277 K using 16% PEG 8 K as the precipitating agent, 0.2 M NaCl and 0.1 M phosphate–citrate buffer pH 4.2. These crystals diffracted up to 3.0 Å resolution using synchrotron radiation (wavelength: 0.979 Å).

The structure of Cld was solved by molecular replacement and it was possible to observe 10 molecules in the asymmetric unit (Fig. 1). These are arranged as two homopentamers with very tight interaction between the five monomers. Each pentamer has a donut-like shape with a maximum outer diameter and height of ~80 Å and ~60 Å, respectively. The five molecules of one homopentamer form an internal cavity with a diameter of ca. 20 Å (Figs. 1 and 2). The quaternary structure was confirmed by determination of the oligomer and monomer masses through size exclusion chromatography (SEC) and MALDI-TOF-MS, respectively. SEC revealed a protein with ~140 kDa while mass spectrometry showed a peak at ~27.8 kDa. These results indicated that both in solution and in the crystal, Cld from *Magnetospirillum* sp. is a homopentamer, as also observed for the Cld from *D. aromatica* RCB [18] and *Candidatus N. defluvii* [17]. A molecular phylogenetic analysis (Fig. S3) performed with the primary amino acid sequence, corroborated that Cld from *Magnetospirillum* sp. must be homopentameric as it belongs to the "long Clds" group [10]. Dimeric Clds like those from *N. winogradskyi* [14], *K. pneumoniae* [20] and *Cyanothece* sp. PCC7425 [21] can be found in a separated branch (Fig. S3).

The low resolution did not allow completing the refinement. However, with the current phases it was possible to distinguish ca. 90% of the residues of the protein. In addition, the present data allowed us to calculate the anomalous maps. Although the X-ray data was

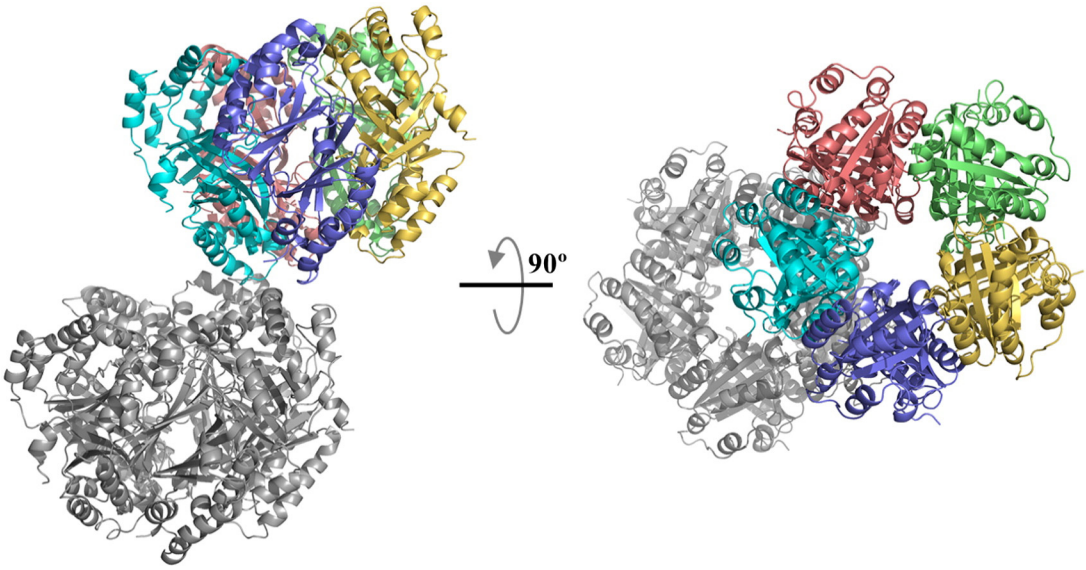

Fig. 1. Overview of the asymmetric unit for Cld crystals from *Magnetospirillum* spp. The right view is rotated 90° from the left view along the horizontal axis shown in the center.

collected far from the iron edge, strong anomalous peaks for the iron atoms were observed in all protein chains, indicating the presence of one *b*-type heme per protein monomer. In order to confirm this observation, Cld purified by any of the two methods described in Section 2.2 were treated according to the alkaline pyridine-hemochrome assay described in Section 2.4. The UV–vis absorption spectrum of the treated Cld samples showed the Soret, α and β bands at 418, 556 and 524 nm, respectively, indicating the presence of the *b*-type heme. Then, correlation of the concentrations of protein, heme and iron, confirmed that Cld from *Magnetospirillum* sp. harbors [0.8 ± 0.1] Fe-heme *per* protein monomer.

In spite of the low resolution of the X-ray data, it was possible to verify that, as observed in the Cld structures of other bacterial sources, the heme cofactors are positioned on the external face of the homopentamer ring (Fig. 2). This orientation may be physiologically relevant as it can promote an easier diffusion of the substrate to the active site and product exit, and this can be correlated with the high turnover rates observed in the kinetic studies (see Section 3.5 below).

An unexpected feature was observed when pure Cld samples were run on polyacrylamide gels under denaturating conditions, as two bands with different mobilities (separated ~2 kDa) were observed (Fig. 3). In order to verify if one of the bands is a contamination, both bands were extracted from the gel. Tryptic digests were obtained for each band (triplicate), and the peptides mix solutions were analyzed by MALDI-TOF-MS. The identification performed by Peptide Mass Fingerprint as described in Section 2.5 revealed that both the upper and lower protein bands (Fig. 3) correspond to Cld. Remarkably, this type of altered electrophoretic mobility was also observed for Cld from *I. dechloratans* [39]. However, in this case a single protein band corresponding to the lower band was observed when Cld was isolated from *Ideonella* cells, while the upper band was observed when the recombinant Cld was heterologously expressed in *E. coli* cells. The authors suggested that the two bands observed in the SDS-PAGE correspond to two forms of the enzyme, which differ in a post-translational modification. It was proposed that the upper band would correspond to the non-modified protein, while the lower band corresponds to a protein modified by an intramolecular covalent cross-link (between His and Tyr side chains), which would only happen in the native organism. In the case of Cld from *Magnetospirillum* sp., the two forms presenting different electrophoretic mobilities were obtained from the Cld purified from the original *Magnetospirillum* cells (Fig. 3). The supposedly non-modified would be the upper band, and the one allegedly modified

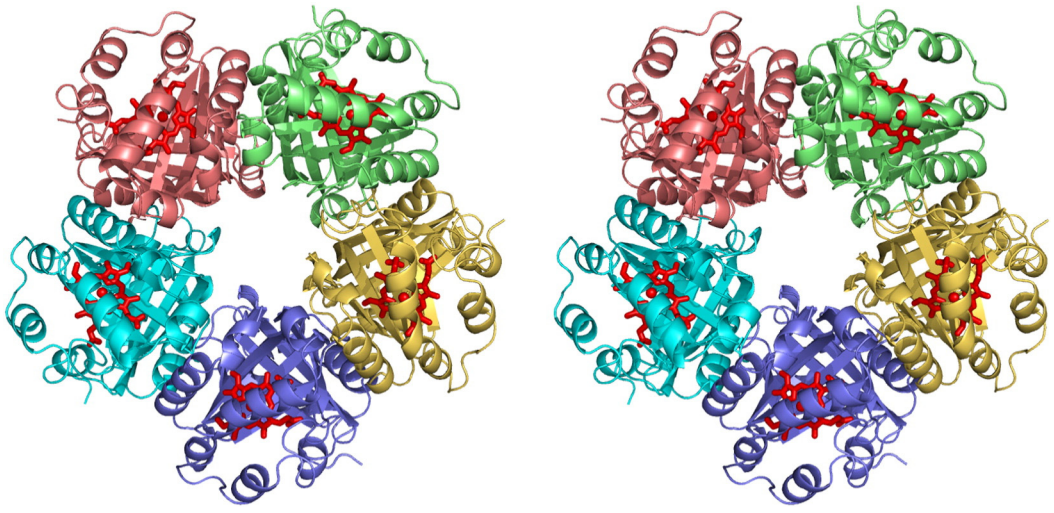

Fig. 2. Stereo view of the Cld pentamer structure. The pentamer is colored by chain and the hemes are shown red. (For interpretation of the references to colors in this figure legend, the reader is referred to the web version of this article.)

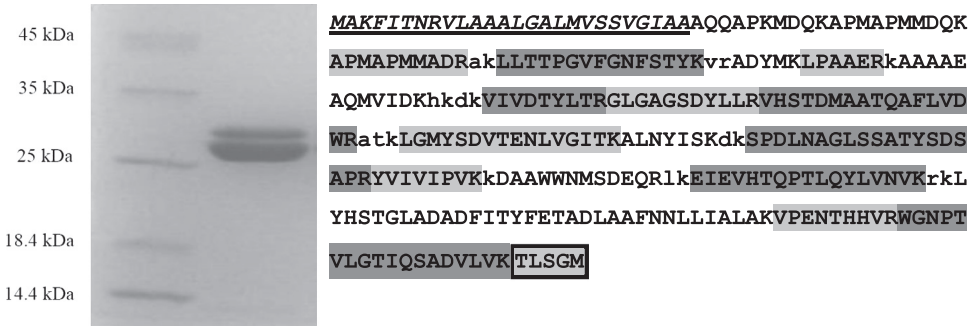

Fig. 3. *Left*: 12.5% SDS-PAGE of pure Cld samples (right lane) and low range molecular mass standards from GE Healthcare (left lane). *Right*: Primary amino acid sequence of *Magnetospirillum* sp. Cld precursor. The signal peptide is shown in italic and underlined and it was predicted using SignalP v4.1 online tool [40]. The assigned peptides obtained by tryptic digestion of both upper and lower protein bands are highlighted in gray. The box indicates a peptide assigned in the upper band but missing in the lower band.

would be the lower band as it migrates faster due (hypothetically) to the smaller hydrodynamic radius of the protein. Although the formation of an intramolecular cross-link would explain the electrophoretic profile, such a bond (or any other post-translational modification that could affect electrophoretic mobility, i.e., glycosylation or myristoylation) was not observed in our preliminary crystallographic results neither in the eight reported Cld crystallographic structures [14,17–19]. On this basis, we considered that the different electrophoretic mobilities of the two bands might be related to proteolysis at the N- and/or C-terminal polypeptide edges. In order to verify this hypothesis, an assignment of the peptides obtained after tryptic digestion was performed (Fig. 3). For our analysis, missed cleavages (up to two), methionine oxidation and potential acrylamide adducts were taken into account. The mature Cld predicted by the online tool SignalP [40] has a molecular mass of ~29.6 kDa (Fig. 3), which is very different from the value ~27.8 kDa obtained by MALDI-TOF-MS of the non-digested Cld. In addition, the predicted mature Cld should generate 21 peptides after tryptic digestion. Unfortunately, only thirteen and twelve peptides could be assigned for the upper and lower protein bands, respectively. The only missing peptide in the lower band (with respect to the upper band) corresponds to the C-terminal edge (indicated with a box in Fig. 3) which would be responsible for a ~0.5 kDa difference. Furthermore, for both upper and lower protein bands, the MALDI-TOF-MS data suggests that mature Cld would start in the amino acid ~47 (APMAPMMADR …), resulting in predicted molecular masses of ~27.5 kDa and ~27.0 kDa, respectively. Although the value predicted for the upper band is close to that of the non-digested Cld (~27.8 kDa), a 0.5 kDa difference could not be solved by the 12.5% SDS-PAGE resolution. Moreover, our X-ray crystallography data showed that in all the polypeptide chains of the asymmetric unit the C-terminal is present and the first observable N-terminal amino acid is the 52, resulting in a predicted molecular mass of ~26.9 kDa, considerably different from the mass of the non-digested Cld. The X-ray crystallography data [14,17–19] plus the analysis presented above, indicate that the electrophoretic profile of Cld from *Magnetospirillum* sp. cannot be explained assuming post-translational modifications and then, this would not have physiological meaning. On the other hand, although proteolysis at the N- and/or C-terminal would explain the different protein bands mobilities, we did not obtain conclusive evidence indicating that this is the case. Taking into account that a single peak is detected by mass spectrometry of pure Cld in solution but two bands are observed in SDS-PAGE, we believe that the modification could be happening during sample treatment (before loading the electrophoresis gel) and the features observed in the SDS-PAGE (Fig. 3) would be a technical artifact.

3.2. UV–vis spectroscopy characterization

The UV–visible absorption spectrum of the as-prepared Cld at pH 6.0 in the presence of air (Fig. 4, solid trace) exhibits a 280 nm protein band (88,000 M^{-1} cm^{-1}), a broad Soret band centered at 392 nm (130,000 M^{-1} cm^{-1}), a broad band with an absorption maximum at 508 nm (21,000 M^{-1} cm^{-1}) and a shoulder at ~535 nm (18,400 M^{-1} cm^{-1}), and a small band at 646 nm (8900 M^{-1} cm^{-1}). The A_{392}/A_{280} ratio (Reinheitszahl) was 1.48. The band centered at 646 nm is typical of Fe^{3+}-heme in high-spin electronic configuration (see inset of Fig. 4, solid trace), in agreement with structural data.

After incubation with sodium dithionite under argon atmosphere (Fig. 4, dotted trace) the Fe^{3+}-heme is reduced to the ferrous state (Fe^{2+}-heme) and the spectrum is characterized by a sharp Soret peak centered at 434 nm, and two smaller peaks at 556 nm and 586 nm (see inset of Fig. 4, dotted trace). When Cld was incubated with sodium ascorbate at equimolar amounts or in large excess no reduction of the heme cofactor was observed, indicating that the midpoint potential of the Fe^{3+}/Fe^{2+} redox couple might be negative (vs. SHE) under the conditions tested (i.e., 50 mM KPB pH 6.0, 298 K). This is in agreement with spectroelectrochemical studies performed with Cld from Candidatus *N. defluvii* and *N. winogradsky* which showed that reduction potentials are in the order of −0.1 V (vs. SHE) and that the Fe^{3+} oxidation state might be enthalpically stabilized [41].

3.3. Influence of the purification protocol in the Cld as-prepared state

The CW-EPR spectra of Cld isolated from *A. oryzae* GR-1, *I. dechloratans* or *D. aromatica* RCB in their as-prepared forms at pH 5.0–7.0 are straightforward to explain [8,15,22]. In these Cld, the EPR signal observable at liquid helium temperatures arises from one high-spin Fe^{3+}-heme species corresponding to the pentacoordinated ferric ion present in the Cld active site. In contrast, Cld from *Magnetospirillum* sp. purified with the protocol using Tris–HCl and MES buffers showed a mixture of at least three high-

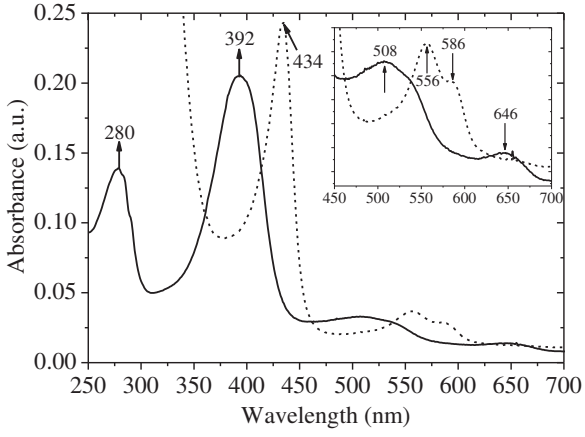

Fig. 4. UV–vis absorption spectra of as-prepared (solid trace) and dithionite-reduced (dotted trace) Cld (~1.58 μM) in 50 mM KPB pH 6.0.

spin species plus one low-spin species which account for ca. 45% of the contribution (Table 2 and Fig. 5A). Due to the large zero-field splitting, the EPR contributions of the high-spin species can be simulated assuming an effective S = 1/2 system with rhombic effective *g*-values (Table 2 and Fig. S4 where it is shown that no remarkable differences are obtained for the simulations performed assuming S = 1/2 or S = 5/2).

Some authors proposed elsewhere that the presence of several paramagnetic species in the EPR spectrum can be correlated with the existence of several bands in the SDS-PAGE. As mentioned in Section 3.1 this would be due to the presence of an intramolecular His-Tyr covalent crosslink [39]. However, as discussed in the same section, we believe that this hypothesis cannot be applied to the case of Cld from *Magnetospirillum* sp. An alternative explanation for the several EPR species observed is that the Cld active site would bind different ligands during the purification process, and these remain in the as-isolated samples. The purification procedure of Cld samples used to trace the spectrum of Fig. 5A included relatively high concentrations of chloride, one of the products of chlorite decomposition. This could be a problem when taking into account that chloride is a mixed inhibitor of Cld with inhibition constants K_{iC} = 460 mM and K_{iU} = 480 mM. Therefore, chloride interacts directly with the active site as well as with another site that affects the structural properties of the catalytic pocket. For this reason, a second batch of Cld was purified but this time, only potassium phosphate buffer was used given that this salt does not affect the Cld activity. The CW-EPR spectrum of Cld purified by the second protocol (Fig. 5B) showed a dominant high-spin Fe^{3+}-heme species (Fe^{3+}: [Ar] $3d^5$, S = 5/2). This signal is identical to those observed in the as-prepared Cld from *A. oryzae* GR-1, *I. dechloratans* or *D. aromatica* RCB at pH values between 5.0 and 7.0 [8,15,22]. Moreover, in this Cld batch no low-spin species were observed (Fig. 5B), supporting the idea that the buffers used during the purification process could influence the heme environment of the as-purified enzyme. Furthermore, SDS-PAGE performed with Cld samples purified by the second protocol also showed two bands in the gel (not shown), confirming that the observation of multiple bands in the SDS-PAGE is not related to the presence of one or several high-spin species in the CW-EPR spectra.

It is clear that the presence of high concentrations of chloride anion in the purification procedure did not affect the presence of the two bands in the SDS-PAGE, though it seems to be involved in the presence of extra paramagnetic species. When a Cld sample is incubated with a saturated NaCl solution, the CW-EPR spectrum is different from that of the as-prepared forms and it is composed of two rhombic Fe^{3+}-heme species in high-spin configuration (Fig. 5C). Interestingly, one of these signals match with one of the smaller high-spin contributions observed in the as-prepared Cld purified through the first protocol, indicating that the chloride anion would remain bound to the heme cofactor after purification and should not be used to isolate this enzyme. Nevertheless, there are other high- and low-spin signals that cannot be explained at present.

Table 2
Simulation parameters for the different Fe(III) contributions to the spectra in Fig. 5.

		Effective S = 1/2			S = 5/2	
	Electron spin configuration	$g_{eff,x}$	$g_{eff,y}$	$g_{eff,z}$	E/D [a]	Relative % versus total Fe(III) contribution
First purification method	High spin	6.72	5.05	1.955	0.0380	9
	High spin	6.29	5.45	1.988	0.0177	45
	High spin	5.97	5.94	2.000	0.0027	1
	Low spin	2.97	2.24	1.47	–	45
Second purification method	High spin	6.72	5.05	1.955	0.0380	6.5
	High spin	6.29	5.45	1.988	0.0177	93.5
Chloride excess	High spin	5.97	5.94	2.000	0.0027	20
	High spin	6.17	5.785	1.998	0.0084	80

Simulations were done in two ways: assuming an effective S = 1/2 system with effective *g* values and assuming an S = 5/2 system with the zero-field parameter D very high (>8 cm^{-1}). In this case, only the E/D ratio can be determined, where E is a measure for the rhombicity of the zero-field tensor. The relative contributions were determined using the S = 5/2 simulation method.

[a] D > 8 cm^{-1}; *g* = [1.97, 1.97, 2].

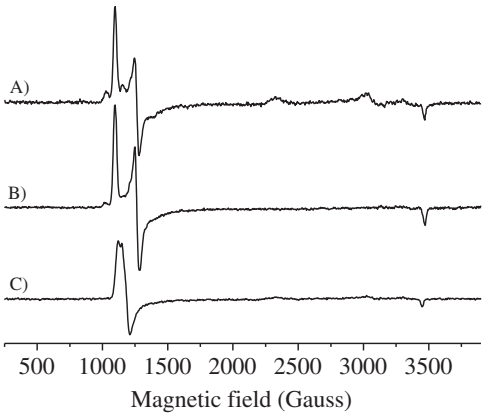

Fig. 5. X-band CW-EPR spectra of Cld from the first (A) and second (B) purification protocols, along with Cld incubated with a large excess of NaCl (C). Cld was at 500 μM in 50 mM KPB pH 6.0 in all cases. EPR measurements conditions are as described in the Materials and methods section.

3.4. Influence of buffer composition on Cld activity

The kinetic characterization of Cld turned out to be challenging because the enzyme catalytic efficiency was remarkably affected by the buffer composition, temperature, pH and ionic strength. For this reason, it was necessary to set the optimal conditions to perform the kinetic assays and obtain reliable kinetic parameters. Buffers of different molecular natures were screened, such as those based on substituted amines (Tris–HCl, Bis–Tris–propane), sulfonate groups (MES, HEPES, CAPS, CAPSO), and inorganic molecules (sodium and potassium phosphate). Amine-based buffers showed a high level of inhibition of Cld activity, while sulfonate-based buffers yielded non-reproducible results. It was determined that potassium phosphate buffer (KPB) did not interfere with the catalytic activity of Cld when used at relatively low concentrations. Therefore, in order to control the pH of the solution, 50 mM KPB was used for the biochemical and spectroscopic characterization.

3.5. Effect of temperature on catalysis

To determine the optimal temperature for Cld activity, steady-state kinetic assays were performed at different temperatures. Unexpectedly, the time courses ([S] vs. time) obtained in the temperature range 5–50 °C showed that the initial rates (slopes) of chlorite reduction were not affected. Nevertheless, it was found that the amount of substrate consumed during the catalysis (i.e., the completeness of the reaction) was dependent on the temperature (Fig. 6). In this regard, full consumption of the substrate was only achieved at low temperatures, more specifically below 10 °C. As the temperature increased above 20 °C it became more evident that the number of catalytic cycles performed decreased while the initial rates were not affected (Fig. 6). This effect was also observed by other authors, that performed the kinetic assays at low temperatures (4 °C) in order to elongate the initial phase of the reaction, although the effect of temperature on reaction completeness was not discussed [16].

As for the temperature, the effect of pressure was evaluated. Since an important fraction of the substrate is not consumed at ~25 °C (Fig. 6), this temperature was used to assess if a considerable pressure variation has an effect on substrate consumption rates and/or completeness of the reaction. However, the kinetic parameters were not affected when the assays were performed at gauge pressures between −1 and 3 bar.

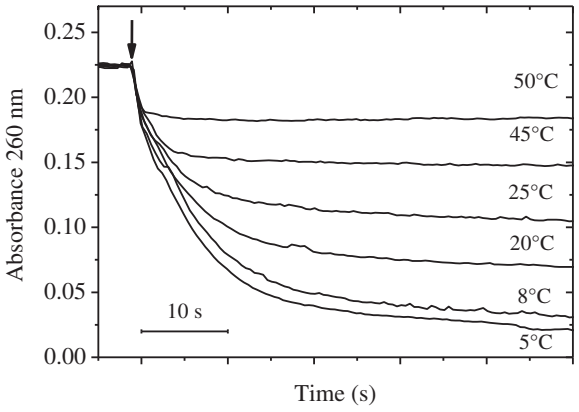

Fig. 6. Time courses ([S] vs. time) of chlorite reduction ($[S]_0 = 1.45$ mM) in 50 mM KPB pH 6.0 in the temperatures range 5–50 °C. The arrow indicates the addition of Cld.

Some authors reported elsewhere [16] that residual chlorite remains after the reaction stopped and that Cld from *D. aromatica* RCB exposed to chlorite loses activity, even after the enzyme is exchanged into fresh buffer. In this case, the authors found that the heme absorbance of the inactivated enzyme disappeared, suggesting heme bleaching and active site destruction. As in that case, we have observed through UV–vis spectroscopy that incubating Cld with a very large molar excess of chlorite also bleaches the heme cofactor, inactivating the enzyme (Fig. S5).

The inactivation observed could not be explained if one of the products (Cl^- or O_2) reacts with the enzyme blocking or destroying the active site. In the case of chloride, we found that this anion is a weak mixed inhibitor of Cld ($K_{iC} = 460$ mM and $K_{iU} = 480$ mM) and dioxygen has no inhibitory effect on Cld, as neither k_{Cat} nor K_M are affected when the kinetic assays are performed either under argon atmosphere ($[O_2] < 0.1$ ppm) or in the presence of air. The fact that dioxygen has no effect on Cld kinetic parameters and the weak mixed inhibitory behavior of chloride were also observed for Cld from *D. aromatica* RCB [16].

Recently, it was demonstrated that during chlorite reduction catalyzed by Cld, hypochlorite is produced during an intermediary stage of the catalytic cycle. The hypochlorite does not react correctly at the Cld active site recombining with the Fe^{IV}=O intermediate, and is released producing oxidative modifications of the protein, leading to heme bleaching and enzyme inactivation [20,42].

3.6. Determination of optimal pH and kinetic parameters

In order to determine the optimal pH for Cld activity several kinetic assays were performed at 5 °C using 50 mM KPB at different pH values. The plot of k_{cat} vs. pH (Fig. 7A) showed that turnover rates are highest at lower pH values, specifically between 5.5 and 6.0. It is also evident that at pH ~7.0 the activity decreases considerably and that at pH ~8.5 the enzyme is virtually inhibited. In order to determine the existence of acid–base transitions that affect the Cld catalytic activity and substrate affinity, a Michaelis–Menten curve was made at several pH values in order to determine the kinetic parameters k_{Cat} and K_M (Fig. S6). The k_{Cat}/K_M ratio was then plotted as a function of the pH and it was observed that the affinity of Cld for chlorite is higher at pH 6.5 (Fig. 7B). Between 6.5 and 7.5 this ratio decreases drastically with a midpoint approximately at pH 6.7. This value might correspond to the acid–base transition of an amino acid residue relevant in substrate binding and/or stabilization that may be located near the active site. Due to the drastic decline of the catalytic activity, the deprotonation of such amino acid residue might have also a key effect in the catalytic properties of the enzyme active site. A similar pKa (6.5) was observed for the Cld from *D. aromatica* RCB [43]. It was proposed that this pKa

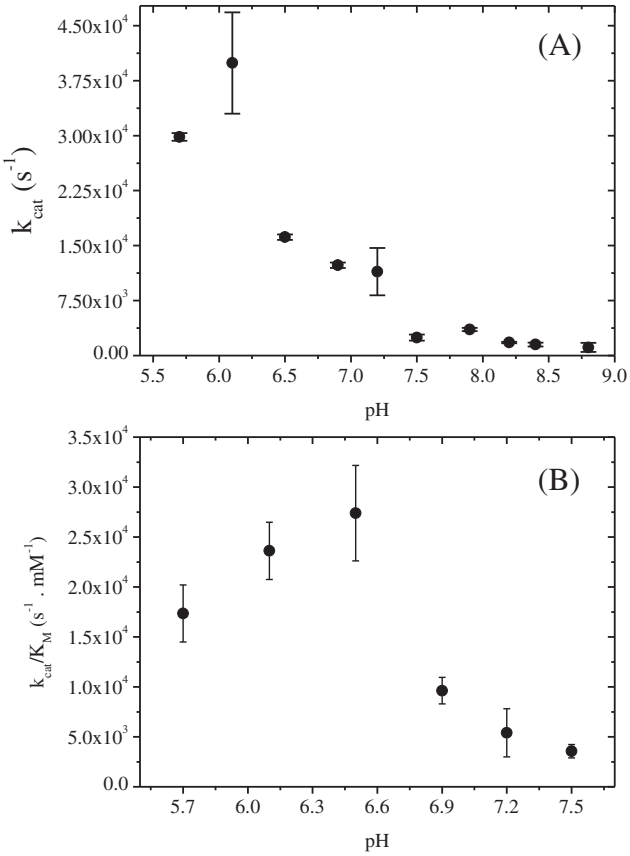

Fig. 7. Chlorite reductase activity as function of the pH. Panels (A) and (B) show the dependence of k_{Cat} (s^{-1}) and the k_{Cat}/K_M ratio (s^{-1} mM^{-1}) versus the pH of the kinetic assay solution, respectively.

would correspond to a change in the availability of positive charge at the distal side of the heme cofactor, due to a conformational rearrangement of the conserved arginine side chain [44]. Taking into account the amino acid sequence similarity and the close phylogenetic distance (Figure S3), this acid–base transition might also be happening in Cld from *Magnetospirillum* sp.

The fact that the maximum affinity ($k_{Cat}/K_M \approx k_{On}$) was obtained at pH ~ 6.5 (Fig. 7B) resulted from the very low K_M value obtained (0.59 mM at pH 6.5 versus 1.7 mM at pH 5.5 and 6.0). On the other hand, the fact that the highest initial rates are obtained at pH values below ~6.0 (Fig. 7A) suggests that protonation of certain amino acid residues near the active site lowers the activation energy barrier of one or several steps of the global reaction mechanism (E_a is directly related to the k_{Cat} through the Arrhenius equation [27]), probably minimizing the electrostatic repulsion between the negatively charged substrate and other groups in the enzyme active site and/or stabilizing intermediaries of the reaction [42].

4. Conclusions

Chlorite dismutase from the (per)chlorate-reducer *Magnetospirillum* sp. was purified for the first time through liquid chromatography using two different protocols which differ in the presence of chloride. This anion affects the EPR signature of the as-prepared Cld samples, and might be a weak ligand of the heme iron (competitive character of the inhibition) and a positively charged neighboring amino acid side chain (uncompetitive character) like the side chain of the Arg residue located at the distal side.

The biochemical studies indicated that Cld from *Magnetospirillum* sp. (purified either in the presence or absence of chloride) is a homopentamer harboring one *b*-type heme per monomer, an

observation that was confirmed by the preliminary X-ray crystallographic structure partially solved at the 3.0 Å resolution. The protein organization and secondary structure of each Cld monomer was determined. The Fe atom of the heme cofactors could be observed in all monomers present in the asymmetric unit thanks to its strong anomalous contribution. On-going research is being performed in order to improve the diffracting quality of the crystals and to obtain high resolution data.

Steady-state kinetic studies in solution showed that Cld is a highly efficient enzyme with kinetic constants close to those reported for Cld from perchlorate-reducing bacteria like *D. aromatica* RCB and *I. dechloratans* (Table 3). In addition, the chloride anion, a product of chlorite reduction, is a weak mixed inhibitor of Cld (Figure S1). On the other hand, dioxygen does not affect the kinetic parameters of Cld.

Cld from *Magnetospirillum* sp. suffers inactivation during turnover at temperatures above 10 °C, as the amount of chlorite that is consumed during the catalysis (i.e., the completeness of the reaction) decreases as the temperature increases (Fig. 6). Other authors demonstrated that during the course of the catalytic cycle, hypochlorite (an intermediary of the reduction of chlorite to chloride) is produced. This oxidizing compound reacts with the protein producing oxidative modifications that leads to heme cofactor bleaching and active site destruction [42]. Since *Magnetospirillum* sp. is cultured at 37 °C, it would be expected that a large fraction of Cld is purified inactive. However, the high turnover rates of Cld compared to that of (per)chlorate reductases [45] would not allow accumulating the very large molar excess needed to observe heme bleaching (Fig. S5). The latter and the use of low temperatures should be taken into account to develop an oxochlorates bioremediation system based on (per)chlorate reductase and chlorite dismutase, the two enzymes responsible for the perchlorate reduction pathway.

Abbreviations

A.	*Azospira*
BCA	bicinchoninic acid
BSA	bovine serum albumin
CAPS	N-cyclohexyl-3-aminopropanesulfonic acid
CAPSO	N-cyclohexyl-2-hydroxyl-3-aminopropanesulfonic acid
Cld	chlorite dismutase
CW	continuous wave
D.	*Dechloromonas*
E.	*Escherichia*
EPR	electron paramagnetic resonance
FPLC	fast performance liquid chromatography
HEPES	4-(2-hydroxyethyl)-1-piperazineethanesulfonic acid
I.	*Ideonella*
ICP-AES	Inductively Coupled Plasma-Atomic Emission Spectroscopy
KPB	potassium phosphate buffer
MALDI	matrix-assisted laser desorption/ionization
MES	2-(N-morpholino)ethanesulfonic acid
MS	mass spectrometry
PAGE	polyacrylamide gel electrophoresis
PEG	polyethyleneglycol
PMF	proton motive force
PRB	perchlorate-reducing bacteria
SDS	sodium dodecyl sulfate
SEC	size-exclusion chromatography
TOF	time of flight
Tris	2-amino-2-hydroxymethyl-propano-1,3-diol

Table 3
Comparison of steady-state kinetic parameters of chlorite reduction by Clds from *Magnetospirillum* sp. and other organisms with reported chlorite-degrading activity.

	pH	K_M (μM)	k_{cat} (s^{-1})	K_{cat}/K_M ($\mu M^{-1}\ s^{-1}$)	Reference
Magnetospirillum sp.	5.7	1720	29,826	17.3	This work
	6.1	1690	39,910	23.6	
	6.5	590	16,157	27.4	
	6.9	1280	12,319	9.6	
	7.2	2120	11,443	5.4	
	7.5	690	2460	3.6	
I. dechloratans	7.0	260	1800	6.9	[15]
D. aromatica RCB	5.2	620	20,000	32	[16,43]
	6.8	212	7500	35	
	7.6	430	3000	6.9	
A. oryzae GR-1	7.2	170	1200	7.1	[13,19,22]
N. defluvii	7.0	69	43	0.6	[17]
N. winogradskyi	7.0	90	190	2.1	[14]
T. thermophilus	7.0	13	0.77	0.059	[46]

Acknowledgments

D.M.F., P.J.G. and C.C. thank Fundação Calouste Gulbenkian for the Programa de Estímulo à Investigação award. P.J.G. and T.S.S. thanks Programa Ciência 2008 of Fundação para a Ciência e a Tecnologia (FCT). This work was supported by FCT through the project POCTI/QUI/55435/2004 and grant no. Pest-C/EQB/LA0006/2011. M.G.R. and P.J.G. are members of CONICET (Argentina). The authors would like to thank the beamline scientists of the ESRF for the assistance in X-ray data collection.

Appendix A. Supplementary data

Supplementary data to this article can be found online at http://dx.doi.org/10.1016/j.jinorgbio.2015.07.006.

References

[1] C.E. Aziz, P.B. Hatzinger, Perchlorate sources, source identification and analytical methods, in: H.F. Stroo, C.H. Ward (Eds.), Situ Bioremediation of Perchlorate in Ground Water, Springer, New York 2008, pp. 55–77.
[2] R.Q. Gullick, M.W. Lechvallier, T.A.S. Barhorst, Occurrence of (per)chlorate in drinking water sources, J. Am. Water Works Assoc. 93 (2001) 66–77.
[3] E.T. Urbansky, Perchlorate chemistry: implications for analysis and remediation, Biorem. J. 2 (1998) 81–95.
[4] G.B. Rikken, A.G.M. Kroon, C.G. van Ginkel, Transformation of (per)chlorate into chloride by a newly isolated bacterium: reduction and dismutation, Appl. Microbiol. Biotechnol. 45 (1996) 420–426.
[5] A. Wolterink, A.B. Jonker, S.W.M. Kengen, A.J.M. Stams, *Pseudomonas chloritidismutans* sp. nov., a non-denitrifying, chlorate-reducing bacterium, Int. J. Syst. Evol. Microbiol. 52 (2002) 2183–2190.
[6] J.D. Coates, U. Michaelidou, R.A. Bruce, S.M. O'Connor, J.N. Crespi, L.A. Achenbach, Ubiquity and diversity of dissimilatory (per)chlorate-reducing bacteria, Appl. Environ. Microbiol. 65 (1999) 5234–5241.
[7] J.D. Coates, L.A. Achenbach, Microbial perchlorate reduction: rocket-fueled metabolism, Nat. Rev. Microbiol. 2 (2004) 569–580.
[8] A.Q. Lee, B.R. Streit, M.J. Zdilla, M.M. Abu-Omar, J.L. DuBois, Mechanism of and exquisite selectivity for O—O bond formation by the heme-dependent chlorite dismutase, Proc. Natl. Acad. Sci. U. S. A. 105 (2008) 15654–15659.
[9] F. Mehboob, A.F. Wolterink, A.J. Vermeulen, B. Jiang, P.L. Hagedoorn, A.J. Stams, S.W. Kengen, Purification and characterization of a chlorite dismutase from *Pseudomonas chloritidismutans*, FEMS Microbiol. Lett. 293 (2009) 115–121.
[10] S. Hofbauer, I. Schaffner, P.G. Furtmuller, C. Obinger, Chlorite dismutases — a heme enzyme family for use in bioremediation and generation of molecular oxygen, Biotechnol. J. 9 (2014) 461–473.
[11] L.M. Dassama, T.H. Yosca, D.A. Conner, M.H. Lee, B. Blanc, B.R. Streit, M.T. Green, J.L. DuBois, C. Krebs, J.M. Bollinger Jr., O(2)-evolving chlorite dismutase as a tool for studying O(2)-utilizing enzymes, Biochemistry 51 (2012) 1607–1616.
[12] B.S. Harrison, D. Eberli, S.J. Lee, A. Atala, J.J. Yoo, Oxygen producing biomaterials for tissue regeneration, Biomaterials 28 (2007) 4628–4634.
[13] C.G. van Ginkel, G.B. Rikken, A.G. Kroon, S.W. Kengen, Purification and characterization of chlorite dismutase: a novel oxygen-generating enzyme, Arch. Microbiol. 166 (1996) 321–326.
[14] G. Mlynek, B. Sjöblom, J. Kostan, S. Füreder, F. Maixner, K. Gysel, P.G. Furtmüller, C. Obinger, M. Wagner, H. Daims, K. Djinović-Carugo, Unexpected diversity of chlorite dismutases: a catalytically efficient dimeric enzyme from *Nitrobacter winogradskyi*, J. Bacteriol. 193 (2011) 2408–2417.
[15] K. Stenklo, H.D. Thorell, H. Bergius, R. Aasa, T. Nilsson, Chlorite dismutase from *Ideonella dechloratans*, J. Biol. Inorg. Chem. 6 (2001) 601–607.
[16] B.R. Streit, J.L. DuBois, Chemical and steady-state kinetic analyses of a heterologously expressed heme dependent chlorite dismutase, Biochemistry 47 (2008) 5271–5280.
[17] J. Kostan, B. Sjöblom, F. Maixner, G. Mlynek, P.G. Furtmüller, C. Obinger, M. Wagner, H. Daims, K. Djinović-Carugo, Structural and functional characterisation of the chlorite dismutase from the nitrite-oxidizing bacterium "*Candidatus Nitrospira defluvii*":

identification of a catalytically important amino acid residue, J. Struct. Biol. 172 (2010) 331–342.
[18] B.R. Goblirsch, B.R. Streit, J.L. DuBois, C.M. Wilmot, Crystallization and preliminary X-ray diffraction of chlorite dismutase from *Dechloromonas aromatica* RCB, Acta Crystallogr. Sect. F: Struct. Biol. Cryst. Commun. 65 (2009) 818–821.
[19] D.C. de Geus, E.A. Thomassen, P.L. Hagedoorn, N.S. Pannu, E. van Duijn, J.P. Abrahams, Crystal structure of chlorite dismutase, a detoxifying enzyme producing molecular oxygen, J. Mol. Biol. 387 (2009) 192–206.
[20] A.I. Celis, Z. Geeraerts, D. Ngmenterebo, M.M. Machovina, R.C. Kurker, K. Rajakumar, A. Ivancich, K.R. Rodgers, G.S. Lukat-Rodgers, J.L. DuBois, A dimeric chlorite dismutase exhibits O2-generating activity and acts as a chlorite antioxidant in *Klebsiella pneumoniae* MGH 78578, Biochemistry 54 (2015) 434–446.
[21] I. Schaffner, S. Hofbauer, M. Krutzler, K.F. Pirker, M. Bellei, G. Stadlmayr, G. Mlynek, K. Djinovic-Carugo, G. Battistuzzi, P.G. Furtmuller, H. Daims, C. Obinger, Dimeric chlorite dismutase from the nitrogen-fixing cyanobacterium *Cyanothece* sp. PCC7425, Mol. Microbiol. 96 (5) (2015) 1053–1068.
[22] P.L. Hagedoorn, D.C. De Geus, W.R. Hagen, Spectroscopic characterization and ligand-binding properties of chlorite dismutase from the chlorate respiring bacterial strain GR-1, Eur. J. Biochem. 269 (2002) 4905–4911.
[23] J.C. Thrash, S. Ahmadi, T. Torok, J.D. Coates, *Magnetospirillum bellicus* sp. nov., a novel dissimilatory perchlorate-reducing alphaproteobacterium isolated from a bioelectrical reactor, Appl. Environ. Microbiol. 76 (2010) 4730–4737.
[24] U.K. Laemmli, Cleavage of structural proteins during the assembly of the head of bacteriophage T4, Nature 227 (1970) 680–685.
[25] K.M. Smith, Porphyrins and Metalloporphyrins, Elsevier Scientific, Amsterdam, Netherlands, 1975.
[26] M. Philippi, H.S. dos Santos, A.O. Martins, C.M. Azevedo, M. Pires, Alternative spectrophotometric method for standardization of chlorite aqueous solutions, Anal. Chim. Acta 585 (2007) 361–365.
[27] A. Cornish-Bowden, Fundamentals of Enzyme Kinetics, 3rd ed. Portland Press, London, 2004.
[28] J. Jancarik, S.H. Kim, Sparse matrix sampling: a screening method for crystallization of proteins, J. Appl. Crystallogr. 24 (1991) 409–411.
[29] A.G.W. Leslie, H.R. Powell, Processing diffraction data with MOSFLM, in: R.J. Read, J.L. Sussman (Eds.),Evolving Methods for Macromolecular Crystallography, vol. 245, Springer, Dordrecht, The Netherlands 2007, pp. 41–51.
[30] P. Evans, Scaling and assessment of data quality, Acta Crystallogr. D Biol. Crystallogr. 62 (Pt 1) (2006) 72–82.
[31] M.D. Winn, C.C. Ballard, K.D. Cowtan, E.J. Dodson, P. Emsley, P.R. Evans, R.M. Keegan, E.B. Krissinel, A.G. Leslie, A. McCoy, S.J. McNicholas, G.N. Murshudov, N.S. Pannu, E.A. Potterton, H.R. Powell, R.J. Read, A. Vagin, K.S. Wilson, Overview of the CCP4 suite and current developments, Acta Crystallogr. D Biol. Crystallogr. 67 (2011) 235–242.
[32] N.m. Collaborative Computational Project, The CCP4 suite: programs for protein crystallography, Acta Crystallogr. D Biol. Crystallogr. 50 (1994) 760–763.
[33] B.W. Matthews, Solvent content of protein crystals, J. Mol. Biol. 33 (1968) 491–497.
[34] K.A. Kantardjieff, B. Rupp, Matthews coefficient probabilities: improved estimates for unit cell contents of proteins, DNA, and protein–nucleic acid complex crystals, Protein Sci. 12 (2003) 1865–1871.
[35] A.J. McCoy, R.W. Grosse-Kunstleve, P.D. Adams, M.D. Winn, L.C. Storoni, R.J. Read, Phaser crystallographic software, J. Appl. Crystallogr. 40 (2007) 658–674.
[36] K.D. Cowtan, DM: an automated procedure for phase improvement by density modification, Joint CCP4 ESF-EACBM Newsl, Protein Crystallogr. 31 (1994) 34–38.
[37] P. Emsley, B. Lohkamp, W.G. Scott, K. Cowtan, Features and development of Coot, Acta Crystallogr. D Biol. Crystallogr. 66 (2010) 486–501.
[38] G.N. Murshudov, P. Skubák, A.A. Lebedev, N.S. Pannu, R.A. Steiner, R.A. Nicholls, M.D. Winn, F. Long, A.A. Vagin, REFMAC5 for the refinement of macromolecular crystal structures, Acta Crystallogr. D Biol. Crystallogr. 67 (2011) 355–367.
[39] H. Danielsson Thorell, N.H. Beyer, N.H. Heegaard, M. Ohman, T. Nilsson, Comparison of native and recombinant chlorite dismutase from *Ideonella dechloratans*, Eur. J. Biochem. 271 (2004) 3539–3546.
[40] T.N. Petersen, S. Brunak, G. von Heijne, H. Nielsen, SignalP 4.0: discriminating signal peptides from transmembrane regions, Nat. Methods 8 (2011) 785–786.
[41] S. Hofbauer, M. Bellei, A. Sundermann, K.F. Pirker, A. Hagmuller, G. Mlynek, J. Kostan, H. Daims, P.G. Furtmuller, K. Djinovic-Carugo, C. Oostenbrink, G. Battistuzzi, C. Obinger, Redox thermodynamics of high-spin and low-spin forms of chlorite dismutases with diverse subunit and oligomeric structures, Biochemistry 51 (2012) 9501–9512.
[42] S. Hofbauer, C. Gruber, K.F. Pirker, A. Sundermann, I. Schaffner, C. Jakopitsch, C. Oostenbrink, P.G. Furtmuller, C. Obinger, Transiently produced hypochlorite is responsible for the irreversible inhibition of chlorite dismutase, Biochemistry 53 (2014) 3145–3157.
[43] B.R. Streit, B. Blanc, G.S. Lukat-Rodgers, K.R. Rodgers, J.L. DuBois, How active-site protonation state influences the reactivity and ligation of the heme in chlorite dismutase, J. Am. Chem. Soc. 132 (2010) 5711–5724.
[44] B. Blanc, J.A. Mayfield, C.A. McDonald, G.S. Lukat-Rodgers, K.R. Rodgers, J.L. DuBois, Understanding how the distal environment directs reactivity in chlorite dismutase: spectroscopy and reactivity of Arg183 mutants, Biochemistry 51 (2012) 1895–1910.
[45] S.W. Kengen, G.B. Rikken, W.R. Hagen, C.G. van Ginkel, A.J. Stams, Purification and characterization of (per)chlorate reductase from the chlorate-respiring strain GR-1, J. Bacteriol. 181 (1999) 6706–6711.
[46] A. Ebihara, A. Okamoto, Y. Kousumi, H. Yamamoto, R. Masui, N. Ueyama, S. Yokoyama, S. Kuramitsu, Structure-based functional identification of a novel heme-binding protein from *Thermus thermophilus* HB8, J. Struct. Funct. Genom. 6 (2005) 21–32.